Experimental investigation of the onset of instability in a radial Hele-Shaw cell

L. M. Martyushev,* A. I. Birzina, M. S. Konovalov, and A. P. Sergeev
Institute of Industrial Ecology, Russian Academy of Sciences, 20A S. Kovalevskaya Street, 620219 Ekaterinburg, Russia
(Received 11 July 2009; published 10 December 2009)

The initial stage of interface instability upon radial displacement of a fluid in a Hele-Shaw cell is investigated. An air-silicone oil system is analyzed. The critical radii of stability relative to long-wave perturbations are determined. It is found that, in the investigated range of parameters, instability most often begins by a translational mechanism. It is ascertained that in the overwhelming majority of cases the critical radii of instability are smaller than the values predicted by the linear stability theory and external effects make this difference even greater. The obtained results are discussed and compared with the existing theories.

DOI: 10.1103/PhysRevE.80.066306 PACS number(s): 47.15.gp, 47.20.Hw

I. INTRODUCTION

Pattern-forming interfacial instabilities have been intensively investigated for quite a long time [1–3]. There are many reasons to that. Among them are the requirements of modern technologies, the interesting and nontrivial theoretical models and approaches considerably enriching our knowledge of the surrounding world, and aesthetic aspects (e.g., amazingly beautiful fractal and dendritic crystal structures resulting from the loss of stability), etc. No doubt, all of the above are also related to the morphological transition, which is the subject of the present work. The paper will discuss a slow quasistationary radial displacement of one fluid by another less viscous fluid in a horizontal cell consisting of two closely arranged plates (the Hele-Shaw cell). The displacing fluid is injected into the cell in its center and, as it moves, at some moment of time the initially round interface of the two fluids loses its stability and gets distorted, transforming to an intricate "fingered" structure.

Also, it is important to consider a system of this kind for the following reasons. Such a transition (in any case, its initial stage) may be quite easily[1] and mathematically accurately modeled and analyzed. At the same time, neither the experimental implementation, nor the investigation of this phenomenon presents any special difficulties. The experiment may be conducted under normal room conditions, without involving special equipment; the phenomenon may be easily reproduced and is observable for many fluids [5–7]. The last circumstance allows investigations to be conducted in a wide range of parameters. The system two-dimensionality required by the theory is easily controllable. The interface between two fluids can be perturbed in many ways when stability is concerned [3,7,8] (for many other, e.g., crystal systems, this is not so simple). Because of these features, the given system proves to be of value from the point of view of not just qualitative, but also quantitative verification of different theoretical approaches and hypotheses. One of such hypotheses is an idea that the loss of morphological stability of the moving interface presents a nonequilibrium phase transition of the first order [3,9,10]. Consequently, a metastable region, in which the morphological transition can be observed, exists. The higher the amplitude of perturbation, the earlier (at smaller sizes of the displacing fluid region) will this transition take place; and vice versa, the lower the amplitude of perturbations, the later will the transition from a round to a distorted displacement front take place in the displacement process, and, respectively, the deeper will the penetration into the metastable region be.

It should be noted that, although theoretical studies dedicated to analysis of the initial stage of transition from a stable to an unstable round interface between two fluids are numerous [9–18], experimental studies are lacking, and, therefore, no attempts have been made at a quantitative comparison with theory at this stage.[2] For this reason, the purpose of this paper was to correct the above fault.

The work is organized in the following way. In the next section, modern theoretical representations of the initial stage of the loss of morphological stability by the moving fluid interface will be outlined briefly. Section III gives a detailed description of the experimental setup, substantiates the selection of fluids for investigation, describes the procedure of analyzing the obtained data (images) and deriving the critical stability radius. Section IV, the core of the paper, presents the obtained results followed by their discussion. The paper ends with the conclusions.

II. THEORETICAL BASIS

The first detailed analytical treatment of radial displacement is found in [11]. The rate of growth of an infinitesimal

*leonidmartyushev@gmail.com

[1]In the majority of cases a linear analysis of interface stability may be sufficient; therewith, the pressure field is well described by the two-dimensional Laplace equation, and all the system parameters are isotropic [4–6].

[2]Experimental studies have been available dedicated mainly to subsequent development of instability: structure fractal dimensionality, competition of emerging "fingers," their rate, shapes, etc. [5–7,11,17–23]. Although this stage of development is of great practical interest, it is the least fortunate from the point of view of verifying and perfecting new ideas and approaches. In fact, mathematical complexity of the object essentially increases here, finally leading to multiple approximations and assumptions. In the long run, both a qualitative and a quantitative comparison with the experimental data get complicated, bringing about great freedom in interpreting the results.

perturbation of a round interface was calculated in linear approximation. The rate of injection of a less viscous fluid through the cell center was assumed to be constant. Both fluids were regarded as immiscible and incompressible. The motion was assumed to be quasi-two-dimensional; i.e., all flow conditions were averaged over the cell thickness. Such an approximation was used in [11], and a similar situation is investigated further in this paper. The cell was regarded as infinite, with a point source of fluid injection. An arbitrarily small distortion of the initially round interface was represented as $r=R+\delta\cos(n\varphi)$, where R is the radial position of the round interface, δ is the perturbation amplitude, n is the azimuthal wave number of the mode, and φ is a polar angle. It follows from the calculation made for the n-th perturbation growth rate that the loss of stability will take place when the interface reaches a critical radius.

$$R_{s,p} = n(n^2-1)\frac{M_1M_2}{M_1+M_2}\frac{2\pi\sigma}{Q}\left(n\frac{M_1-M_2}{M_1+M_2}-1\right)^{-1}, \quad (1)$$

where $M_i=b^2/12\mu_i$, μ_i is the fluid viscosity, b is the distance between the cell plates, ($i=1$, 2 for the displacing or the displaced fluid, respectively), σ is the surface tension, Q is a constant flow rate (mm^2/s). When this size is exceeded, the perturbation growth rate changes sign from negative (perturbation damping) to positive (perturbation development).

Although the calculations made in [11]. permitted a qualitative description of the phenomena observed in the experiment, they had a number of drawbacks. First, the result Eq. (1) tells nothing of what is likely to happen with the so-called translational perturbation[3] ($n=1$). Second, the solution was sought based on an assumption of a pressure jump at the two fluids interface described by the Laplace formula $2\sigma/b+\sigma K$, where K is the interface curvature in the plane of motion. Obviously, this classical equilibrium condition presents a rather rough assumption for the problem considered. Third, the paper gives no indication of how the loss of stability would occur if the interfaces perturbation were noninfinitesimal. In particular, would the critical stability radius determined by Eq. (1) decrease, increase, or remain unchanged.

As distinct from [11], account was taken in [13]. of finiteness of the sizes: the Hele-Shaw cell R_∞ and the hole through which the fluid was injected R_0. Taking into account the boundaries allowed predicting the existence of a critical radius of stability for the perturbation growth at the wave number $n=1$. According to estimates, if the viscosity of the displacing fluid is much lower than the viscosity of the displaced fluid ($M_2/M_1\sim 10^{-3}$), translational instability will most probably be observed in the experiment.

The Laplace condition for the problem considered was given a more accurate definition in [24]. It was assumed that the displaced fluid completely wetted the walls, leaving a thin film on the walls while being displaced. An analysis yielded the following approximate formula for the pressure jump, $2\sigma/b+\alpha V^\gamma+\beta K$, where $\alpha=7.6\sigma(\mu_2/b)^\gamma/b$, $\beta=\pi\sigma/4$, $\gamma=2/3$ and V is the fluid velocity. This condition manifestly accounts for the influence of the fluid motion rate on the interface shape (second term), and a correction is introduced to account for a change in the interface shape across the cell thickness (third term). The critical stability radius R_s relative to the n-th harmonic, accounting for this condition in the linear order of the perturbations theory, as is shown in [14] [4], may be found by numerically solving the equation

$$1+n\left(\frac{M_2}{M_1}-1\right) \times \frac{1+\left[(n^2-1)\frac{\beta}{R}-\alpha\gamma\left(\frac{Q}{2\pi R}\right)^\gamma\right]\frac{2\pi}{Q}\frac{M_1M_2}{M_2-M_1}}{\frac{M_2}{M_1}\frac{1+(R_0/R)^{2n}}{1-(R_0/R)^{2n}}+\frac{1-(R/R_\infty)^{2n}}{1+(R/R_\infty)^{2n}}+n\alpha\gamma\left(\frac{Q}{2\pi R}\right)^\gamma\frac{2\pi M_2}{Q}} = 0. \quad (2)$$

A detailed analysis of this solution and the peculiarities emerging in such description of displacement is given in [14]. It should be noted only that, with the specified conditions at the interface taken into account, the stability radius becomes much smaller (by tens of percent) than the value found earlier [11,13]. Considering perturbations at $n=1$, Eq. (2) allows the critical radius to be determined in an explicit form:

$$R_{S,1} = R_0\sqrt{\frac{(M_2/M_1)(R_\infty/R_0)^2+1}{1-M_2/M_1}}. \quad (3)$$

It is worth noting that in this case the critical radius turns out to be independent of the rate of displacement and the distance between the cell plates.

A linear analysis for morphological stability fails to answer where the critical stability radius would shift if the perturbation amplitude were noninfinitesimal. At the same time, from the point of view of practice and experimental check of theoretical predictions [including Eqs. (1)–(3)], this question is topical, since, in a real experiment, one can hardly expect the perturbations to be of an exclusively infinitesimal kind. A study of the influence of noninfinitesimal perturbations on stability of radial displacement in the Hele-Shaw cell was made in [15,16]. In these papers, a weakly nonlinear analysis of the problem was carried out. A second order mode coupling differential equation for the perturbation amplitudes was derived. It was also shown that the interaction of modes is the underlying factor of "fingers" branching.

Reference [9] proposes a hypothesis that, with an increase in the amplitude of perturbations, the critical radius will decrease to a size determined by solving the following equation relative to R:

[3] According to [11], the perturbation growth rate ($n=1$) is always negative at $R>0$.

[4] An allowance for such a corrected Laplace condition is also made in [19,20], on the assumption of a constant pressure at the cell entrance, but not of the injected fluid stream.

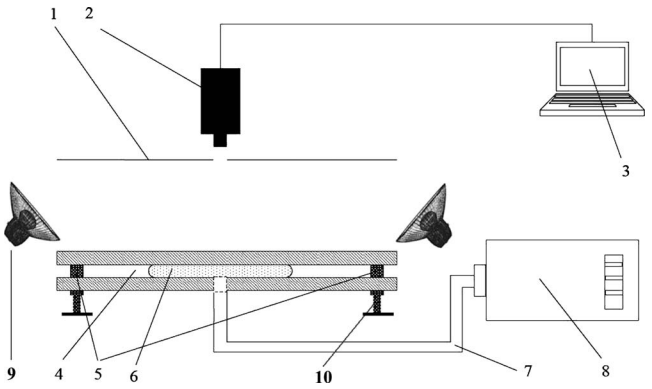

FIG. 1. Experimental setup (Hele-Shaw cell). 1—light-diffusing screen; 2—digital video camera; 3—personal computer; 4—glass plates; 5—spacers; 6—displaced fluid; 7—pipe for displacing fluid injection; 8—low-rate compressor; 9—light source, 10—adjustment bolts fixed on a stable base to exclude influence of vibrations etc.

$$\left(\frac{Q}{2\pi R}\right)^2 + \frac{Q}{\pi} M_2 R^{n-1} a_2 n[1 + (R_\infty/R)^{2n}] = 0, \qquad (4)$$

where a_2 is a sufficiently complicated function[5] depending on R and the other parameters responsible for displacement. This conclusion is based on entropy production calculations and the so-called maximum entropy production principle (see [3,25,26]). The interval between the radius determined from Eq. (4) and R_S is referred to as metastable.

Thus, it follows from the above considerations that the theory predicting the behavior of the interface between two fluids in a Hele-Shaw cell at the initial stage of stability loss has been developed in sufficient detail. At the same time, no experimental measurements enabling either quantitative confirmation or disapproval of the above results may be found in the literature.

III. EXPERIMENTAL PROCEDURE

A. Experimental Setup

The experimental setup schematic is shown in Fig. 1. The central component of the experimental setup was the so-called Hele-Shaw cell presenting two planar-parallel plates from transparent float glass: the lower glass $600 \times 600 \times 10$ mm in size, and the upper glass shaped as a circle 500 mm in diameter and 10 mm thick. The glass plates were arranged horizontally, at some distance one from the other ensured by metallic spacers of varying thickness. The cell spacing was uniform to within ± 0.01 mm (on account of the upper glass deflection by gravity). For each test, the plates were leveled (to within $0.057° = 1$ mm/m). With this tilt, the characteristic rate of the fluid flow by gravity only was not over 10^{-4} mm^2/s, which was much less than the investigated displacement rate ($\sim 10^2$ mm^2/s). The bottom plate of the cell had a hole 4 mm in diameter for connecting a pipe to inject the displacing fluid. The hole edges were smoothed and polished to avoid strong perturbations of the injected fluid at inlet. As a result, the actual diameter of the hole, at which a radial displacement started, was 11 mm. The fluid was injected using an original compressor whose working chamber volume was varied by a piston moving at a constant velocity. This provided an almost constant controlled flow rate in the range of 0.05 to 2 ml/s.

At the beginning of the experiment the whole cell was slowly filled with silicone oil. The absence of air bubbles and other impurities was controlled visually. The experiment consisted in silicone oil displacement with air from a bubble 11 mm in size (of 5.5 mm radius) to a bubble with a pronounced loss of stability by the boundary (the process was video recorded). Then the air bubble was withdrawn back to the size of 11 mm (i.e., system returned to the initial state). Several initial cycles of this kind were preparatory to exclude the effect of microroughness formed after preliminary cleaning of the glass surfaces of the cell.

In each experiment the rate and constancy of the flow were controlled by analyzing the video images (see next section). Quasi-two-dimensional structures formed by the fluid injected in the cell were recorded with the help of a Panasonic digital video camera (NV-GS500) with a 3xCCD (charged-coupled device); 1/4.7″ matrix (each CCD matrix providing a 1.07 Mpix resolution). The quality of the video images was improved: (1) for higher contrast, with a black mat film reducing the intensity of flares applied on the lower plate of the Hele-Shaw cell; (2) with a white screen installed to reflect and diffuse the light directed on it from below. The video record was transmitted in the digital form to a personal computer for further processing.

A system of air and silicone oil (polymethyl siloxane fluid, PMS-5 in the Russian classification) was taken for investigating the loss of interface stability. Air is traditionally selected as the displacing fluid for reasons of simplicity in implementation of experiments. Silicone oil (PMS-5) was chosen from the following considerations: (1) oil wets very well the glass used for the plates, leaving a thin uniform film while being displaced[6]; (2) silicone oil viscosity is relatively low $M_2/M_1 \approx 4 \cdot 10^{-3}$ (compared with, e.g., glycerin); consequently, the critical stability radii must be larger, facilitating their study with an acceptable accuracy without magnification; (3) the physical and chemical parameters of this oil weakly depend on temperature and are known to sufficient accuracy (see Table I) ([27]); (4) in compliance with the technical standard (GOST 13032–77 in Russian), silicone oil of the given grade is free from mechanical impurities, water mass fraction being not over 0.004%. It was necessary to account for the above conditions, since the purpose was to carry out a quantitative comparison with the theory based on a number of assumptions (in particular, good wettability of the cell with the displaced fluid).

B. Analysis of Images

We analyzed all images extracted from the video data (the spatial resolution of the images was 9216 pixel/in^2; the rate

[5]Its explicit form may be found in [9].

[6]Water, for example, wets glass quite poorly and leaves no film upon displacement, while castor oil leaves a film of uneven thickness.

TABLE I. Selected properties of silicone oil (PMS-5) [27].

PMS-5 $(CH_3)_3SiO$-[-$Si(CH_3)_2O$-]$_k$-$Si(CH_3)_3$, k is a medium degree of molecules polymerization	
Molecular mass	690
Density, kg/m^3, at 300 K	910
Dynamic viscosity, 10^{-3} Pa·s, at 300 K	4.368
Surface tension, 10^{-3} N/m	18.1
Temperature viscosity coefficient, ratio of viscosity at 360 K to viscosity at 300 K	0.41

of image acquisition was 25 frames/s). Figure 2 depicts several images observed in one of the experiments.

For processing of the experimental results (images from video files), a program module was created in the MATLAB software with the use of the image processing toolbox. The module task was to determine the initial moment of the interface transition from a round to the so-called "fingered" geometry.

The program module sequentially performed the following functions:

(1) Discriminating the two-phase interface. This was done using the Canny Method by searching for local areas with jumps in brightness (Fig. 3).

(2) Filling the object internal area with black pixels and calculating the digitized figure area by counting the number of black pixels in the image (Fig. 4). Conversion to system units was done using round templates preliminarily recorded at the beginning of the experiment.

(3) Plotting the interface from the polar angle (the hole for fluid injection is taken as the center). Further, the moving-average method was used to remove the noise connected with digitization discreteness [Fig. 5(a)]. In every experiment, to correct the distortions caused by tilting of the video camera, we video recorded an array of round templates of different known sizes drawn beforehand in the graphic package and printed out. Further, by comparing the obtained template image and the known template parameters (the dependence of the radius on the angle was analyzed), a correction coefficient was found to account for the appearing distortion. Using this coefficient, the interface images obtained in the experiment were corrected [Fig. 5(b)]. The correction coefficient was introduced taking into account the size of the air bubble.

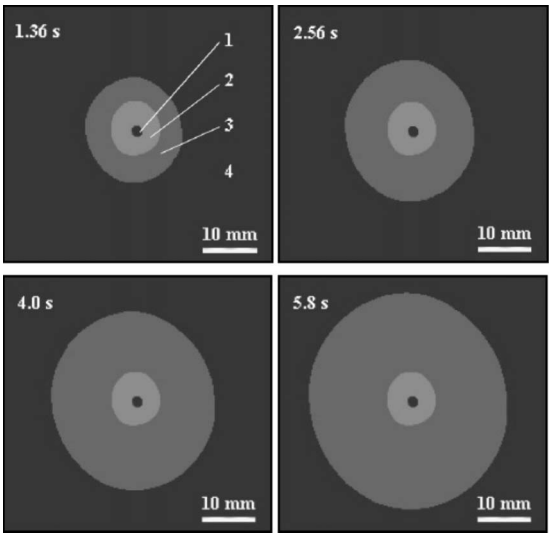

FIG. 2. Four frames of the air bubble growth before processing. 1—hole for injection of the displacing fluid, 2—polished area (actual size of the radial displacement onset), 3—displacing fluid (air), 4—displaced fluid (silicone oil). Q=230.4 mm^2/s, b=0.6 mm.

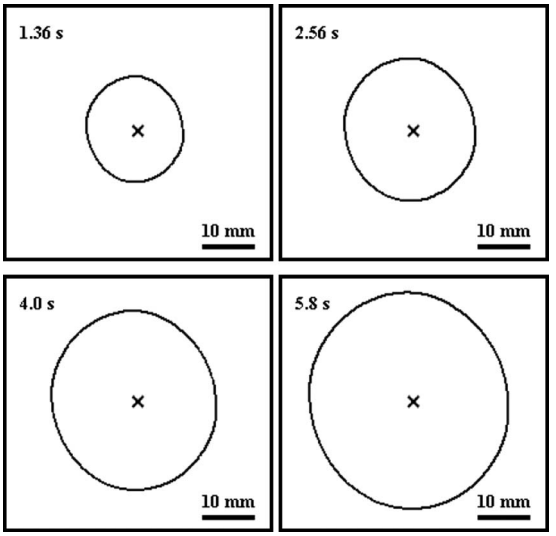

FIG. 3. Four frames presented in Fig. 2 after preliminary processing (binarization, noise reduction and edge extraction).

(4) Fourier series expansion of the obtained function of the polar angle (Fig. 6). The variation of the Fourier coefficients with time allows the interface evolution to be traced and, particularly, the critical stability radius to be defined. In defining this radius, it is necessary to take into account an error arising from the fact that, in digital recording of an image, the position of the center of displacement and the two-phase interface may be defined to a one-pixel accuracy only. To account for this error, the following operations were performed in processing of each image: (1) regarding the center coordinates as a random variable distributed normally within a circle with a center specified by the user and a radius equal to an image discretization unit value (pixel); (2)

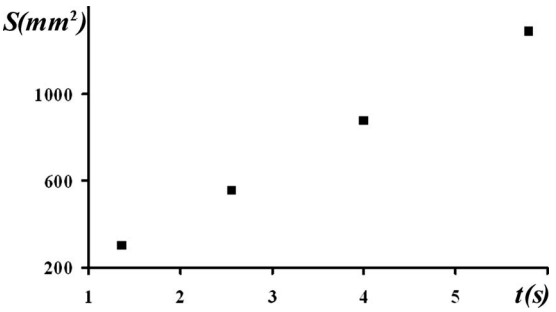

FIG. 4. Spot area S as a function of time t during the air bubble growth, for frames presented in Fig. 2

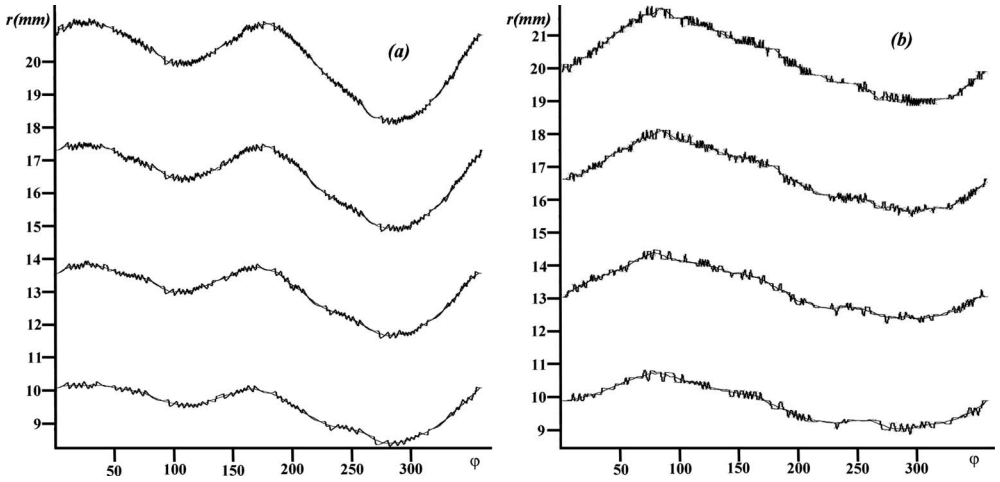

FIG. 5. Distances from the center r as a function of the polar angle φ: (a) before accounting for distortions caused by tilting of the camera, (b) after such accounting. Plotted for frames presented in Fig. 2.

representation of the interface as a region up to three pixels thick, and random selection of the interface coordinate within this region (in this case, a number of conditions should be fulfilled for the "generated interface," namely, the absence of self-intersections, one-pixel thickness, etc.). As a result, a great number of boundaries with such randomization were obtained for each image (10 in this study), and a great number of Fourier coefficients could be calculated. Their averaged value with an error was used as the final value (see Fig. 6). Naturally, such forced measures led to largely inaccurate final results, allowing only long-term tendencies in coefficients variation to be determined. Clearly, this approach led to some overestimation of the confidence interval (particularly, translational distortions of the interface), resulting, among other things, in that the time of the reliable variation of the Fourier coefficients was overrated a little. For this reason, the true stability loss radius for one or the other harmonic must not exceed the determined value.

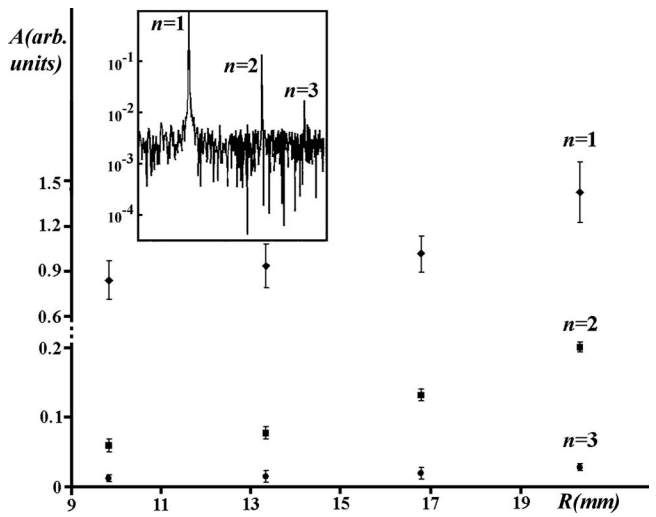

FIG. 6. Dependence of the first three Fourier coefficients A_n on a zero coefficient of Fourier series (A_0) corresponding to the radius R of the moving phase boundary. Plotted for frames presented in Fig. 2. The broader the confidence interval, the greater are the values of the initial radius (the bubble growth time) from which the Fourier coefficients variation may be established reliably. For example, if there were no confidence interval, then, apparently, for the case presented in Fig. 6, at $n=1$, the value of 13.3 mm, and not 20.3 mm, would be critical. The insets show an example of Fourier spectra at $R=16.8$ mm.

The created software module was tested using templates placed on the Hele-Shaw cell lower glass and video recorded. The video camera settings corresponded to the subsequent experiments. The templates were circles of different radii, with added known sinusoidal perturbations (Fig. 7). The results obtained for circles with the radius R not over 50 mm[7] and perturbation amplitudes δ from 1 to 10% of the radius are as follows.

(1) Mode $n=1$. These are most difficult to determine in terms of quantity. The maximum error for small radii and small amplitudes may be up to 700%. As the radius and the perturbation amplitude increase, the error incurred in the amplitude becomes significantly smaller (down to 10%). At the same time, the method displays a change in the translational harmonic amplitude both in the case of varying δ/R and in a more complicated case of $\delta/R=$const. A numerical implementation of the Fourier transform also "reveals" higher wave number harmonics, which are absent in the template. However, the amplitude of these harmonics is more than one order of magnitude lower than that of the harmonic with $n=1$, while their value varies ambidirectionally and more than one order of magnitude slower as compared with variation in the first harmonic amplitude.

(2) Mode $n=2$. These harmonics are somewhat easier to determine quantitatively than those above. For small radii and low perturbation amplitudes, the error is also maximum (up to 50%), but it reduces to 3% with increasing radius and amplitude. At the same time, the method reliably registers variation of the second harmonic amplitude. Numerical calculation reveals false harmonics. While the harmonics with a wave number $n\geq 3$ have an amplitude several times smaller

[7]As the experiment shows (see Sec. IV), it is up to this size that the loss of stability takes place in the investigated system.

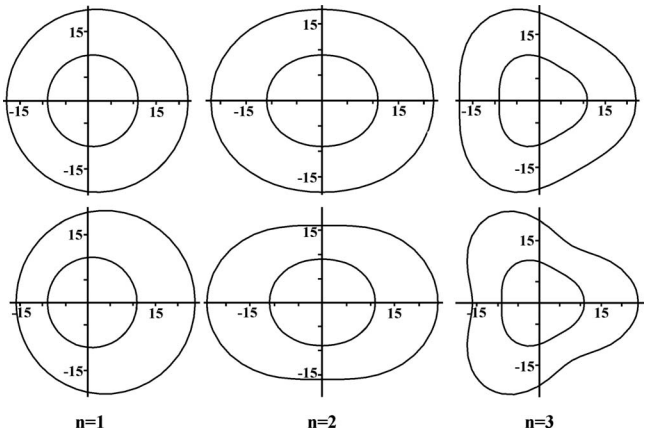

FIG. 7. Examples of circles with superimposed sinusoidal perturbations $n=1$, $n=2$, and $n=3$. In the top line, the sinusoidal amplitude accounts for ten percent of the circle radius ($\delta/R=$const); in the bottom line, the smaller circle is drawn with the sinusoidal amplitude of $0.1R$, and the larger one, with the perturbation amplitude of $0.2R$.

than those with $n=2$, the amplitude of the harmonic with $n=1$ may be much larger (especially at small radii and low perturbation amplitudes). However, variation of these false harmonic amplitudes is ambidirectional, and it is at least one order of magnitude smaller than the variation of the amplitude of the harmonic with $n=2$.[8]

(3) Mode $n=3$ and over. The results were found to be much similar to those in the second case.

Thus, testing demonstrated that for bubbles (of the radius R not over 50 mm) the variation (growth or decay) of distortions (to an amplitude beginning from 1% of the radius) can be reliably registered. No quantitative conclusions on the value of interface distortions can be made from the image analysis module used in the work. Therefore, in this paper, the Fourier coefficients are plotted in Fig. 6 and further not in absolute, but in arbitrary units.

C. Determination of the Critical Radius

The experimental results were processed as follows:

(1) The frames captured from video files were processed following the algorithm described in Sec. III B.

(2) Usually, some time was required for the displacement rate to become constant after the setup was energized. Therefore, for control of the constant flow rate (air injection to the cell), the time dependence of the air bubble area (see Fig. 8) was checked for linearity. The points (generally, at the very beginning and, sometimes, at the end of the experiment) deviating from linearity were rejected until the coefficient of correlation between the experimental points and the straight line was higher than 0.999. The frames corresponding to rejected points were excluded from processing. If the above

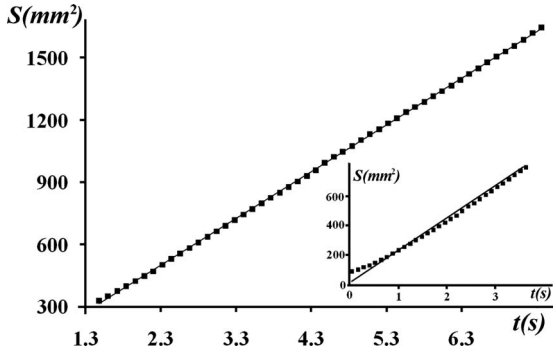

FIG. 8. Variation of the air bubble area S with time t. The inset shows the initial nonstationary part, which will be disregarded in further analysis.

criterion could not be satisfied (or the number of the remaining points was too small), the experiment was viewed as flow unsteady and ignored.

(3) In stationary experiments, dependences of the first three harmonics amplitudes on the growing air bubble radius (in essence, this is a zero coefficient of the Fourier series) were plotted. These dependences (see, e.g., Fig. 9) served to determine the radius, at which the harmonic at hand began growing (to be precise, this critical radius was assessed from top). The method is clear from Fig. 9. This radius corresponds to the minimum abscissa of a point on the curve, whose confidence interval does not overlap with the confidence interval of the points at the beginning of the curve.

(4) Some experiments at the same parameters were conducted. In each experiment, stability loss radii were found for each of the three harmonics. Then the radii found in each experimental series were averaged, and their confidence interval was determined. It was already noted that the value found by this method represented a limiting and, evidently, a slightly overstated estimate.

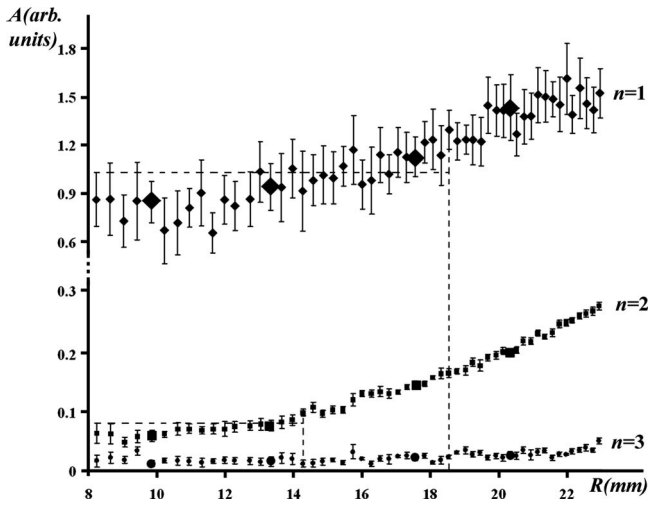

FIG. 9. Variation of the amplitude of the first three harmonics of the Fourier expansion A_n vs radius. Large symbols correspond to frames presented in Fig. 2. Other comments can be found in the text.

[8]An exception is low perturbation amplitudes (1%), when δ/R remains constant as the second harmonic increases. In this case, the harmonic with $n=1$ grows just two times slower than the first harmonic ($n=2$).

TABLE II. Summary of measurement results

Number of experiments	Q (mm^2/s)	b (mm)	n	R_{ex} (mm)	$R_{s,p}$ (mm) [Eq. (1)]	R_s (mm) [Eqs. (2) and (3)]
7	123.0 ± 0.4	0.60 ± 0.03	1	18.2 ± 1.2		17.2
			2	16.8 ± 1.0	38.6	30.3
			3	38.5 ± 1.6	76.9	60.4
4	226.6 ± 1.2	0.60 ± 0.03	1	20.4 ± 0.9		17.2
			2	15.2 ± 0.9	21.0	16.5
			3	34.9 ± 1.3	41.7	32.8
10	230.6 ± 0.3	0.60 ± 0.03	1	17.6 ± 1.3		17.2
			2	13.2 ± 0.7	20.6	16.2
			3	23.8 ± 1.0	41.0	32.2
7	83.9 ± 0.6	0.80 ± 0.03	1	9.8 ± 0.7		17.2
			2	8.8 ± 1.3	100.6	77.5
			3	11.3 ± 0.7	200.3	150.4
7	162.2 ± 1.0	0.80 ± 0.03	1	11.3 ± 0.7		17.2
			2	9.6 ± 0.7	52.0	40.8
			3	13.0 ± 0.9	103.6	81.3

IV. RESULTS AND DISCUSSION

The values of the critical stability radii R_{ex} are given in Table II. The same table lists values of the critical stability radius calculated from Eqs. (1) and (2).

An analysis of the available data suggests the following conclusions.

(1) Translational instability ($n=1$) is observed upon displacement in experiment. This fact is inconsistent with the theoretical predictions given [11], stating that this type of instability should not be observed. The reason is that the finite size of the Hele-Shaw cell was neglected in the calculations. Indeed, the data for $n=1$ vary little from the theoretical prediction in Ref. [14], where this contribution was taken into account.

(2) The critical stability radii found experimentally at $n=2$ and $n=3$ are much smaller than the values predicted in both [11,14]. As regards the critical radius at $n=1$, no such unambiguous conclusion can be made. However, if we recall that the experimental values were overestimated, it can be concluded that in the case of translational instability the experiment also gives values not larger than those predicted by the theory [14].

(3) We cannot but note that the stability radii found for different harmonics n are quite close one to the other (especially at $b=0.8$ mm). A probable explanation of this fact is that the surface harmonics do not develop independently. No prediction with regard to the above observation was offered in [11–14] dealing with the linear perturbation theory. However, according to the weakly nonlinear theory, such a dependence can be observed if perturbations are not infinitesimal [15,16,28]. Experimental results allow us to presume the existence of a mutual dependence in the development of the first harmonics. Probably, the wider the cell gap, the stronger is the harmonics mutual interaction, and, hence, the loss of stability by one of the harmonics (the first one in our case) leads to avalanche-like loss by the rest.

Thus, according to the results described above, the actual radii of interface stability are smaller than the values predicted by the linear theory. It has been noted in the foregoing (Sec. II) that a linear analysis permits establishing stability only with respect to infinitesimal perturbations, and it cannot provide information whether the transition would be sub or supercritical if the perturbation were noninfinitesimal. Since in real conditions perturbations of different amplitudes will always be present, it can be concluded that a subcritical transition will take place in the displacement process at hand. To what extent can the values, at which the transition from a round to a fingered interface occurs, be smaller than the values predicted by the linear theory? In other words, what the width of the metastable region is? We attempted to tackle this problem in relation to translational instability caused by the shift distortion. The procedure was as follows. When the cell was filled with the displaced fluid, the upper glass was shifted 10 mm relative to the center. Then the compressor was started, and displacement began. As soon as the beginning of growth of the air bubble was detected visually, the upper glass was reset to its original position. The time of the shift was 0.3 to 0.4 s. As a result, the air bubble shifted relative to the center and stretched a little (see Fig. 10). According to measurements, subsequent to an abrupt increase caused by the shift, the perturbation corresponding to $n=1$ continued growing. Correspondingly, the experimental values of the critical stability radius upon the shift approximately corresponded to the air bubble radii at the moment the external effect was removed. Oppositely, subsequent to the shift that caused an abrupt increase in the second and third harmonic amplitudes, these amplitudes decreased at a fairly fast rate (see Fig. 11). The experimental data are given in Table III.

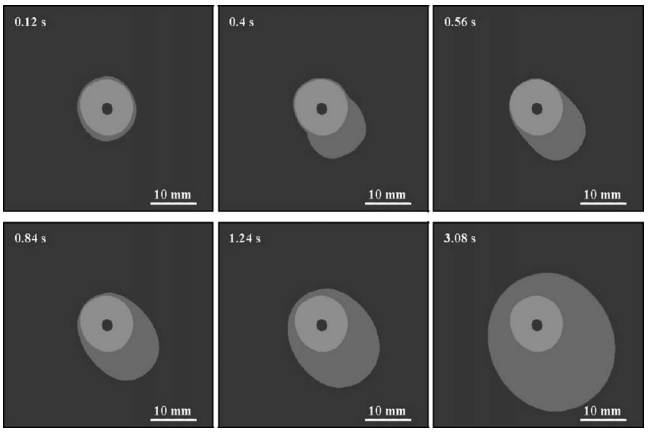

FIG. 10. Six frames of the air bubble growth under the action of the shift. The second frame (0.4 s) corresponds to the moment of the shift. Q=159.7 mm^2/s, b=0.8 mm.

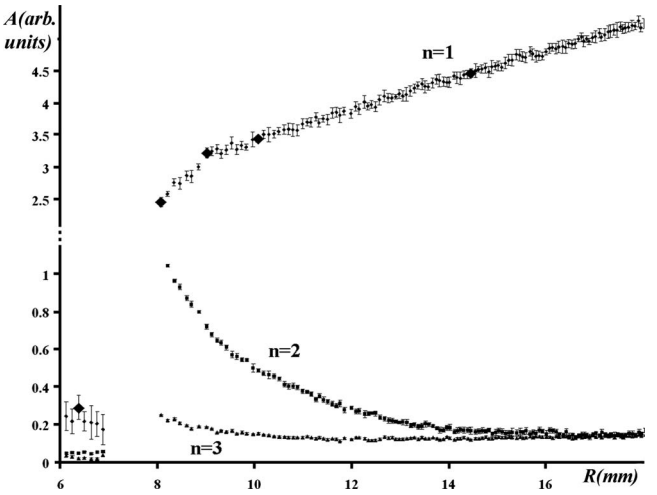

FIG. 11. Variation of the amplitude of the first three harmonics of the Fourier expansion A_n vs. the radius under the action of the shift. Large symbols correspond to the frames presented in Fig. 10.

A comparison of the respective R_{ex} values listed in Tables II and III suggests a conclusion that the first harmonic development under the shift takes place at earlier stages. This is most evident in the experiments at $b=0.6$ mm. A probable explanation is that in any experiments, including those shown in Table II, the presence of noninfinitesimal perturbations cannot be excluded. When $b=0.8$ mm, these perturbations result in that loss of stability by the first harmonic takes place at sizes of 9.8–11.3 mm (Table II). These values are quite close to those minimum possible (5.5 mm). For this reason, introduction of auxiliary (shift) perturbations decreases little the value of loss of stability. At $b=0.6$ mm, the critical values are considerably larger (17.6 mm) than those minimum possible, and, correspondingly, the shift results in a more significant change of the critical radius.

Thus, perturbation shifts the critical radius at $n=1$ to smaller values, decreasing it approximately two times as compared with the radius predicted by the linear perturbation theory [14]. According to the measurements, this value is the smaller, the shorter the shift time (see Table III). This is due to the fact that the loss of stability is detected immediately after the perturbing effect has been removed; and the shorter the shift time, the smaller is the air bubble growth. To all appearance, if the shift velocity is increased, a situation is possible when the critical radius upon the shift ($n=1$) approaches the radius of the hole for injection of air. In our case, its radius is 5.5 mm. It is interesting to note that, according to the predictions in [9] (see also Eq. (4)), the metastable region for the first perturbation mode is always found in the interval from 5.5 to 17.2 mm under the experimental conditions in Table III. This fact is an argument in favor of the theory assuming the presence of metastable regions upon displacement in the Hele-Shaw cell; it also supports the method proposed for calculation of these regions [9]. For a more reliable substantiation of this conclusion, the metastable region boundaries should be compared with those predicted theoretically for perturbations at $n>1$.

V. CONCLUSION

An experimental setup was used for quantitative investigation on the initial stage of loss of stability upon a radial displacement of the fluid in a Hele-Shaw cell. Two basic results can be highlighted:

(1) In the silicone oil-air system studied, the presence of a translational mechanism responsible for the loss of morphological stability was detected at the displacing fluid flow rate from 80 to 230 mm^2/s and the cell thickness of 0.6−0.8 mm. This fact and a quantitative comparison of the experimentally obtained and theoretically predicted values suggest that the theory accounting for finite sizes of the Hele-Shaw cell [14] is most suitable for description of real experiments.

(2) It was found that in the majority of cases critical stability radii prove to be smaller than the values predicted by the linear stability theory. In other words, the morphological transition from a round to a distorted interface takes place

TABLE III. The critical radii of stability relative to translational perturbations ($n=1$) caused by the shift distortion

Number of tests	Q (mm^2/s)	b (mm)	Time of shift (s)	R_{ex} (mm)	$R_{s,1}$ (mm) [Eq. (3)]
9	159 ± 1	0.80 ± 0.03	0.32 ± 0.03	9.8 ± 0.7	
6	83 ± 1	0.80 ± 0.03	0.28 ± 0.05	9.0 ± 1.0	17.2
8	236 ± 2	0.60 ± 0.03	0.43 ± 0.04	11.8 ± 0.7	

earlier than it follows from the theory assuming an infinitesimal amplitude of the interface perturbation. Since in any, even most accurate, experiment uncontrolled effects (perturbations), including noninfinitesimal ones, cannot be excluded, we come to a conclusion that the value of perturbation influences the position of the transition point, reducing the critical radius. Introduction of external translational perturbations, as was done in this work, confirms this conclusion: the loss of stability in response to the introduced perturbation is observed practically at once; i.e., the critical radius approaches the minimum possible value. The metastable interface behavior upon displacement in a radial Hele-Shaw cell, which was established in this work, is very important for development of the theory of subcritical nonequilibrium transitions.

ACKNOWLEDGMENTS

The authors wish to thank D. A. Gorchakov for assistance. This work was supported in part by the Russian Foundation for Basic Research (Grant No. 070800-139).

[1] H. Haken, *Synergetics* (Springer, New York, 1978), p. 419.
[2] G. Nicolis and I. Prigogine, *Exploring Complexity: An Introduction* (W.H. Freeman, New York, 1989), p. 313.
[3] E. Ben-Jacob and P. Garik, Nature (London) **343**, 523 (1990).
[4] D. Bensimon, L. P. Kadanoff, S. Liang, B. I. Shraiman, and T. Chao, Rev. Mod. Phys. **58**, 977 (1986).
[5] P. G. Saffman and G. I. Taylor, Proc. R. Soc. London, Ser. A **245**, 312 (1958).
[6] G. M. Homsy, Annu. Rev. Fluid Mech. **19**, 271 (1987).
[7] J.-D. Chen, Exp. Fluids **5**, 363 (1987).
[8] K. V. McCloud and J. V. Maher, Phys. Rep. **260**, 139 (1995).
[9] L. M. Martyushev and A. I. Birzina, J. Phys.: Condens. Matter **20**, 465102 (2008).
[10] E. Álvarez-Lacalle, J. Ortín, and J. Casademunt, Phys. Rev. Lett. **92**, 054501 (2004).
[11] L. Paterson, J. Fluid Mech. **113**, 513 (1981).
[12] S. D. R. Wilson, J. Colloid Interface Sci. **51**, 532 (1975).
[13] L. M. Martyushev and A. I. Birzina, Pis'ma Zh. Tekh. Fiz. **34**, 71 (2008) [Tech. Phys. Lett. **34**, 213 (2008)].
[14] L. M. Martyushev and A. I. Birzina, J. Phys.: Condens. Matter **20**, 045201 (2008).
[15] J. A. Miranda and M. Widom, Physica D **120**, 315 (1998).
[16] E. Álvarez-Lacalle, E. Pauné, J. Casademunt, and J. Ortín, Phys. Rev. E **68**, 026308 (2003).
[17] M. J. P. Gingras and Z. Racz, Phys. Rev. A **40**, 5960 (1989).
[18] L. Paterson, Phys. Fluids **28**, 26 (1985).
[19] A. Buka, P. Palffy-Muhoray, and Z. Racz, Phys. Rev. A **36**, 3984 (1987).
[20] E. Ben-Jacob, G. Deutscher, P. Garik, N. D. Goldenfeld, and Y. Lareah, Phys. Rev. Lett. **57**, 1903 (1986).
[21] M. Sastry, *et al.*, Curr. Sci. **81**, 191 (2001).
[22] S. N. Rauseo, P. D. Barnes, and J. V. Maher, Phys. Rev. A **35**, 1245 (1987).
[23] S. B. K. Burns and S. G. Advani, Exp. Fluids **21**, 187 (1996).
[24] C.-W. Park and G. M. Homsy, J. Fluid Mech. **139**, 291 (1984).
[25] L. M. Martyushev and V. D. Seleznev, Phys. Rep. **426**, 1 (2006).
[26] L. M. Martyushev, V. D. Seleznev, and I. E. Kuznetsova, Zh. Eksp. Teor. Fiz. **118**, 149 (2000) [JETP **91**, 132 (2000)].
[27] P. G. Alekseev, I. I. Skorokhodov, and P. I. Povarnin, *Properties of Organic Silicone Liquids. Handbook* (Energoatomizdat, Moscow, 1997).
[28] L. M. Martyushev, E. M. Sal'nikova, and E. A. Chervontseva, Zh. Eksp. Teor. Fiz. **125**, 1128 (2004) [JETP **98**, 986 (2004)].